Journal of
Nanoscience and Nanotechnology
Vol. 6, 2354–2361, 2006

Investigation of Sisal Fibers by Atomic Force Microscopy: Morphological and Adhesive Characteristics

F. L. Leite[1,2], P. S. P. Herrmann[1], A. L. Da Róz[3], F. C. Ferreira[4], A. A. S. Curvelo[3], and L. H. C. Mattoso[1,*]

[1] Embrapa Agricultural Instrumentation, P.O. Box 741, 13560-970, São Carlos, São Paulo, Brazil
[2] Institute of Physics of São Carlos, University of São Paulo, 13560-970, São Carlos, São Paulo, Brazil
[3] Institute of Chemistry of São Carlos, University of São Paulo, 13566-590, São Carlos, São Paulo, Brazil
[4] University of State of São Paulo, 19060-900, Presidente Prudente, São Paulo, Brazil

Atomic force microscopy (AFM) was used to study the nanoscale surface chemistry and morphological changes caused by chemical treatment of sisal fibers. Scanning Electron Microscopy (SEM) micrographs indicated that sisal *in natura* (bundle of fibers) is formed by fibers with diameters of approximately 10 μm. AFM images showed that these fibers consist of microfibrils with diameters varying from 250 to 600 nm, which are made up of nanofibrils of ca. 20 nm in diameter. The adhesion force (pull-off force) between the AFM tip and the fibers surface increased after benzylation, pointing to a decrease in the polar groups on the sisal fiber. The adhesion map measured over a scan range of 3 μm was heterogeneous in samples treated with 40% NaOH and the low adhesion sites disappeared after benzylation. Using an established mathematical model, it was possible to evaluate the increase in adhesion work and consequently in the interaction between the AFM tip and sisal fibers. These results indicated that AFM can detect heterogeneity in the wettability of sisal fibers with nanometer resolution and can be applied in the study of fiber-matrix adhesion in polymer composites.

Keywords: Atomic Force Microscopy, Force Curve, Adhesion, Sisal Fibers, Wettability, Benzylation, Morphology, Composites.

1. INTRODUCTION

Plant fibers have been employed in a wide range of manufacturing applications, such as in the textile, paper, automobile and chemical industries, and as reinforcement in composites to create materials with improved performance.[1,2] The replacement of synthetic fibers by natural ones, e.g., sisal fibers, is attractive owing to environmental issues. Sisal fiber is composed of 12% polyoses, 14.5% extractives, 1.7% ash, 12.6% lignin, which is a complex polyphenolic material, and 65% cellulose,[3] a linear polymer of anhydroglucose units. These units contain three hydroxyl groups, which lead to the formation of intramolecular and intermolecular hydrogen bonds. Therefore, sisal fibers have a hydrophilic nature, which makes it difficult the interaction with synthetic non-polar matrices. Chemical treatments can be employed to decrease the content of hydroxyl groups, consequently reducing the fiber polarity. One of such possible treatments is benzylation[4–6] used for conversion of vegetal biomass into thermoplastic materials due to the substitution of hydroxyl by benzyl groups, which promotes separation of the cellulose chains by preventing hydrogen bonding. Iannace et al.[7] investigated the physicochemical properties and surface modification of sisal fibers applied in composite materials. Nair et al.[8] studied polystyrene reinforced with sisal fibers and concluded that subjecting the fibers to benzylation improved the fiber-matrix adhesion, increasing the resistance to traction. In composite materials, sisal fibers have already been used as reinforcement in several matrices, such as epoxy,[9,10] polypropylene[11] and polyethylene.[12]

Contact angle analysis may be used to characterize the heterogeneity in the wettability of sisal fibers and to corroborate pull-off force data. It consists in depositing a solvent drop, with well-known values of surface tension, on a flat surface and observing the angle formed between the surface and the drop. There are various approaches to evaluating the surface energy, including the Owens-Wendt

*Author to whom correspondence should be addressed.

 1533-4880/2006/6/2354/008 doi:10.1166/jnn.2006.522

theory.[13] In this theory it is assumed that the polar and non-polar components of surface energy can be combined as a geometric mean:

$$w_{sl} = \gamma_l(1+\cos\theta) = 2\sqrt{\gamma_s^d \gamma_l^d} + 2\sqrt{\gamma_s^p \gamma_l^p} \quad (1)$$

where w_{sl} is the work of adhesion between the solid (s) and the liquid (l), θ is the contact angle, γ^p and γ^d are the polar and non-polar (dispersive) components, respectively. Dividing Eq. (1) by $2\sqrt{\gamma_l^d}$:

$$\frac{\gamma_l(1+\cos\theta)}{2\sqrt{\gamma_l^d}} = \sqrt{\gamma_s^d} + \sqrt{\frac{\gamma_l^p}{\gamma_l^d}}\sqrt{\gamma_s^p} \quad (2)$$

Hence, a graph of $\gamma_l(1+\cos\theta)/2\sqrt{\gamma_l^d}$ versus $\sqrt{\gamma_l^p/\gamma_l^d}$ leads to a straight line with intercept $\sqrt{\gamma_s^d}$ and angular coefficient equal to $\sqrt{\gamma_s^p}$, which are the values of surface energy of the material. Measurements of contact angle have been used in cellulosic materials,[14] phenolic resins[15] and glass fibers,[16] although this technique also has been rarely exploited in the surface energy study of plant fibers or of sisal fiber.

A complete understanding of the surface chemistry and morphology of sisal fibers requires the use of characterization techniques with access to the nanoscale, as is the case of AFM,[17, 18] which has been used to investigate surface properties of polymers[19, 20] cellulose,[14] wool fibers,[21] Kraft pulp fibers,[22, 23] wood-pulp fibers[24] and paper.[25] With AFM, one can explore the chemical heterogeneity, wettability and adhesiveness of sisal fibers on the micro and nanoscale under ambient conditions, particularly probing effects from chemical treatments of the fibers. In this paper, we describe the adhesive and morphological properties of sisal fibers *in natura* and chemically modified using AFM (supplemented by SEM). We also study effects from surface modification of the fibers.

2. EXPERIMENTAL DETAILS

2.1. Samples

Sisal fibers (*Agave sisalana*) were supplied by Icomar (São Paulo, Brazil). Cells of the parenchyma of sisal fibers were partly removed by extraction, in a Soxhlet apparatus, with cyclohexane/ethanol (1:1 v/v) for 22 hours. Alkali treatments were performed by placing 1.0 g of sisal fiber in a flask and adding 17.5 mL of NaOH 40% aqueous solution. The reaction was maintained under constant mechanical stirring for 1 hour at a temperature of 110 °C. The benzylation reactions were carried out by mixing 1.0 g of dried sisal fiber with 17.5 mL of NaOH 40% aqueous solution and 7.5 mL of benzyl chloride at 110 °C, for 0.5 and 2 h, respectively, under constant mechanical stirring. The product of this reaction was washed with ethanol and distilled water to eliminate residues of excess reagent and salt, respectively, removed by extraction in a Soxhlet apparatus.[5]

2.2. Atomic Force Microscopy (AFM)

The morphology of the sisal fiber and their adhesive characteristics (pull-off force) were obtained with a Topometrix TMX 2010 Discoverer and were analyzed using WSxM (Nanotec Electronica S.L.) free software downloadable at http://www.nanotec.es. The rectangular cantilevers of silicon nitride had a spring constant, $k = 0.06 \pm 0.01$ N/m and a tip with radius of curvature, $R_t = 60 \pm 7$ nm. The length (L), width (W) and thickness (t) of the cantilever and the radius of pyramidal tip were measured with a SEM, model XL30-FEG Philips.[26] The cantilever elastic constant was calculated with the following equation:

$$k = EWt^3/4L^3 \quad (3)$$

where $E \sim 1.7 \times 10^{11}$ N/m^2 is the Young's modulus of the cantilever.[27]

The shape of the tip end is critical for the identification of imaging artifacts. In addition, the precise knowledge of the tip radius is required for calculation of surface energy and work of adhesion. Conventional SEM can identify the overall tip shape but with a limited spatial resolution and the requirement of a metal coating reduces its usefulness for AFM tips with radii below 100 nm. To estimate the tip radius with higher resolution, we employed the SPIP™ (Scanning Probe Image Processor) Characterizer. The simulation of the shape and radius of curvature of the tip are shown in Figure 1a. The results obtained from the simulation are consistent with the data from SEM (Fig. 1b). Scan sizes of 1.5 μm $\times$1.5 μm were measured, the images were divided into 512×512 pixels resulting in lateral resolution of 2.93 nm/pixel. Various numerical procedures for the extraction of the tip shape information have been proposed ranging from deconvolution by using mathematical morphology formalism to simple analytical expressions assuming a spherical shape for the tip end.[28, 29]

The roughness parameters were calculated using Scanning Probe Image Processor (SPIP) version 3.1.0.1 from Image Metrology A/S 2003. Describing surface roughness involves measurement of asperity height and distribution of an index of surface roughness. Asperity height is typically made along a straight line across the surface, which yields a two dimension (2-D) profile. By closely spacing a series of profile lines, a three-dimensional (3-D) representation of the surface can be obtained. The surface roughness is quantified by two parameters of roughness: average roughness (R_a) and root-mean square roughness (RMS). The first represents an average of the asperity heights (absolute value) along a centerline defined as a line separating equal areas enclosed by the profile above and below the line, as can be seen in Figure 2. The second parameter frequently used is the root-mean square roughness (RMS), which is essentially the standard deviation of the asperity heights above and below the datum. These parameters are defined by Eqs. (4) and (5),

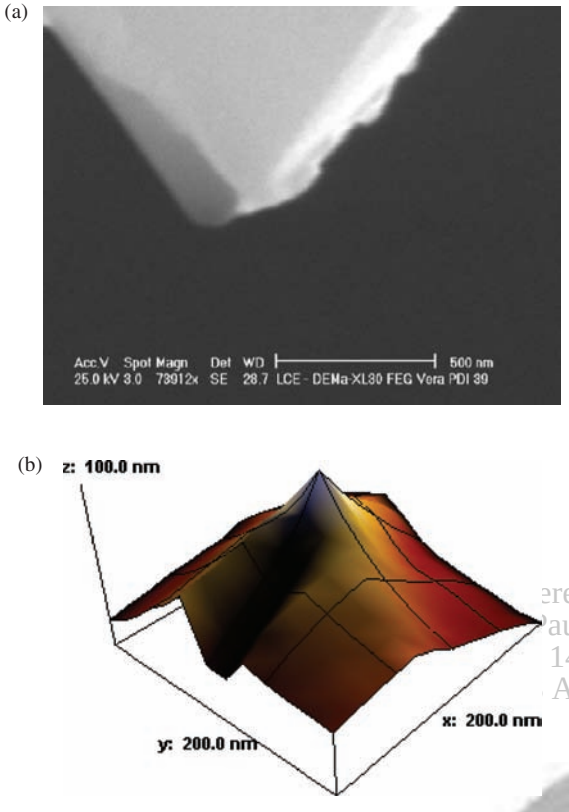

Fig. 1. Tip characterization. (a) radius of curvature estimated by SPIP Characterizer—tip radius (50 ± 3) nm and (b) Micrograph of the silicon nitride AFM tip with radius of $R_t = (60 \pm 7)$ nm.

respectively:[30]

$$R_a = \frac{1}{L}\int_0^L |F(x)|dx \tag{4}$$

where $F(x)$ is the profile height above datum and L is the sampling length.

$$\mathrm{RMS} = \left(\frac{1}{L}\int_0^L F(x)^2 dx\right)^{1/2} \tag{5}$$

2.3. Contact Angle Measurements

One of the experimental techniques used to quantify the surface properties of solids is the contact angle measurements of liquids on solid surfaces. Contact angle can be used simply as an empirical parameter to quantify the wettability. This analysis was performed from pellets similar to those used in infrared spectroscopy, with surfaces as flat as possible. The equipment used was built in the laboratories of Ecole Française de Papetèrie et des Industries Graphiques as described by Aurenty et al.[31] The liquids used were water, formamide, diiodomethane and hexadecane, whose surface tensions are 72.2, 58.3, 50.8, and 27.6 mJ/m^2, respectively. The surface energies and their polar and non-polar components were calculated by Owens-Wendt theory using Eqs. (1) and (2).

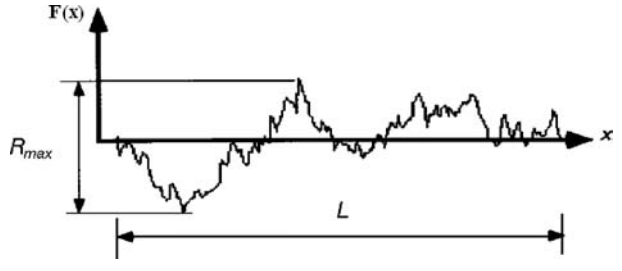

Fig. 2. Definition of parameters to describe surface roughness. R_{max} is the maximum distance between the highest point and the lowest point on the profile.

2.4. Scanning Electronic Microscopy (SEM)

Morphological analysis by SEM was performed with a Zeiss DSM 960 computerized microscope (Jena, Germany) operating between 10 and 20 kV on samples containing a thin layer (ca. 15 nm) of sputter-coated gold.

3. RESULTS AND DISCUSSION

The effects from chemical treatments on the morphology of sisal fibers are shown in the SEM images of Figure 3. Cells of the parenchyma, present in the sisal fiber *in natura* (Fig. 3a), were partly removed by the extraction with organic solvent (results not shown) used before the alkaline treatment. While extraction with organic solvents did not result in any changes in the morphology of the sisal fiber, alkali treatment caused a partial delignification. A small separation is observed between the fibers (diameters of ca. 10 μm) due to the partial removal of lignin and polyoses present in the middle lamella (Fig. 3b). This means that alkali treatment will render the hydroxyl groups at the fiber surface more susceptible to the attack of other chemical agents. Figure 3c shows the micrograph of the fiber benzylated for 0.5 hour. The reaction of benzylation occurs in alkaline solution, which facilitates attack on the cellulose oxygen by the benzyl groups. Figure 3c shows the beginning of the surface modification of the fibers due to the introduction of the benzyl groups in the cellulose chains. Although 0.5 hour benzylation reaction promotes modifications on the fiber surfaces, they do not lose significantly their fibrillar structure. However, Figure 3d shows that after 2 hours of benzylation the fibrillar structure is lost.

The AFM images in Figure 4 indicate that the sisal fibers consist of aligned microfibrils. The effect of benzylation (0.5 hour of reaction) on the morphology of the sisal fiber surface is shown in Figure 4b, where the microfibrils have developed a globular formation. The globules have a relatively uniform size, maintaining in their organization a fibrillar form about the same magnitude as the microfibrils of sisal treated with 40% NaOH. It is known that the benzylation reaction initiates at the surface of the sisal fibers, extending to their interior as the reaction proceeds. This may be the reason why the initial fibrillar structure is not

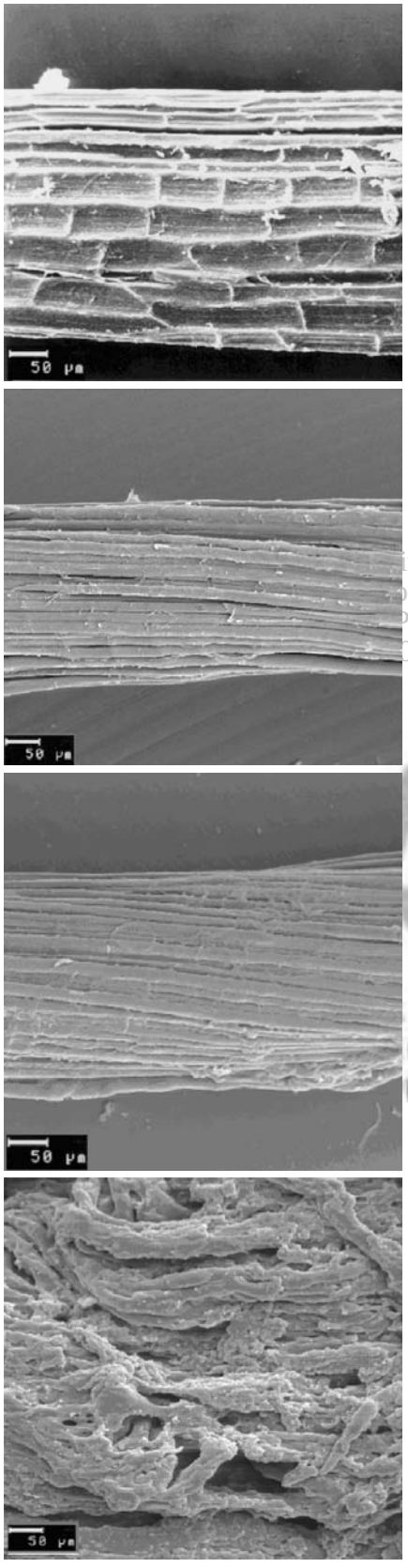

Fig. 3. SEM micrographs (200×) of sisal fiber (a) *in natura*; (b) treated with 40% NaOH; (c) benzylated for 0.5 and (d) 2 hours.

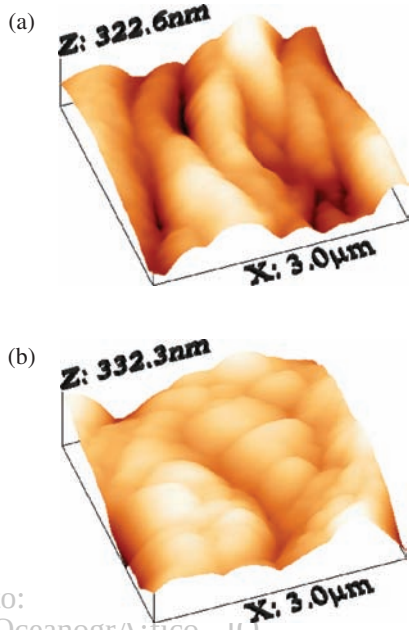

Fig. 4. 2D AFM images of microfibrils (a) treated with 40% NaOH and (b) benzylated for 0.5 hour.

lost (Fig. 3c) after 0.5 hour benzylation, although surface modifications are observed at a smaller scale (Fig. 4b).

Figure 5 shows 2D AFM images of morphological changes with different benzylation times. The fiber treated with 40% NaOH (Fig. 5a) has a fibrillar structure; after 0.5 hour of benzylation a globular structures appear without destroying the fibrillar appearance (Fig. 5b). However, after a longer time (e.g., 2 hours) of benzylation the fibrillar structure is lost, as indicated by the globular morphology in Figure 5c. From section analysis, the diameter (d) of the microfibrils is estimated to lie within 250–600 nm, in agreement with Ref. [32].

The size of the globules on the benzylated sisal is around 100–350 nm. The heights of both fibers and globules were also measured, and a decrease was observed after benzylation, also indicated in the roughness values. The values of the apparent heights (ΔZ) were between 58 and 98 nm for the sisal fiber treated with 40% NaOH and between 25 and 47 nm for the sisal fiber benzylated for 0.5 h. The measured dimensions of the sisal fibers varied with the experimental scanning parameters, such as scanning speed, area scanned and feedback circuit, in addition to the elastic

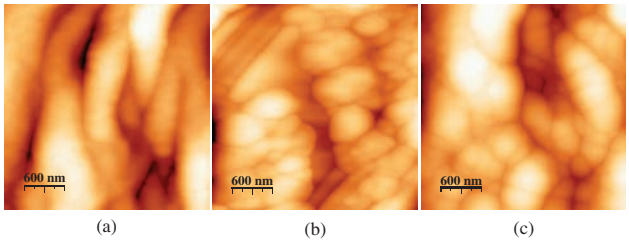

Fig. 5. 3D AFM images (scan size: 3 μm). (a) Treated with 40% NaOH; (b) benzylated for 0.5 hour and (c) for 2 hours.

properties. It is difficult to obtain precise height values for the fibers owing to the roughness and to limitation of the Z piezo. Thus the experimental results of ΔZ and d might differ to some extent from the actual values.

The roughness of sisal fiber treated with NaOH 40% was 21.5 nm (R_a) and 29.7 nm (RMS), which decreased after benzylation for 0.5 hour to 15.3 nm and 19.5 nm, respectively. The roughness of sisal fiber treated with NaOH 40% was higher than the benzylated fiber due to initial de-structuring of the fibril, resulting from the extraction of lignin and polyoses. However, upon incorporation of benzyl groups the roughness is decreased because the material becomes more amorphous.[5] The data for roughness from line analysis were similar to those obtained with area analyses, where R_a and RMS also decreased from 17.1 nm (R_a) and 23.5 nm (RMS) to 13.6 nm and 11.5 nm, respectively, after benzylation.

The intermittent contact mode (Nanoscope IIIa AFM) was also used to study the sisal fibers. The sensitivity of the phase to detect surface features and compositional variations has made phase imaging an appropriate mode for studying fiber surfaces.[33] Figure 6a shows the phase image of a fiber after alkali treatment, which is formed by microfibrils. However, in a higher magnitude the phase image (Fig. 6b) revealed that the microfibrils are constituted by nanofibrils with diameters of approximately 20 nm. These values are consistent with the microfibrils shown in wood chemistry books, e.g., Ref. [34]. In summary, a sisal fiber *in natura* consists of a bundle of fibers (Fig. 3b) that contain aligned microfibrils (Fig. 5a) formed by several randomly distributed nanofibrils (Fig. 6b).

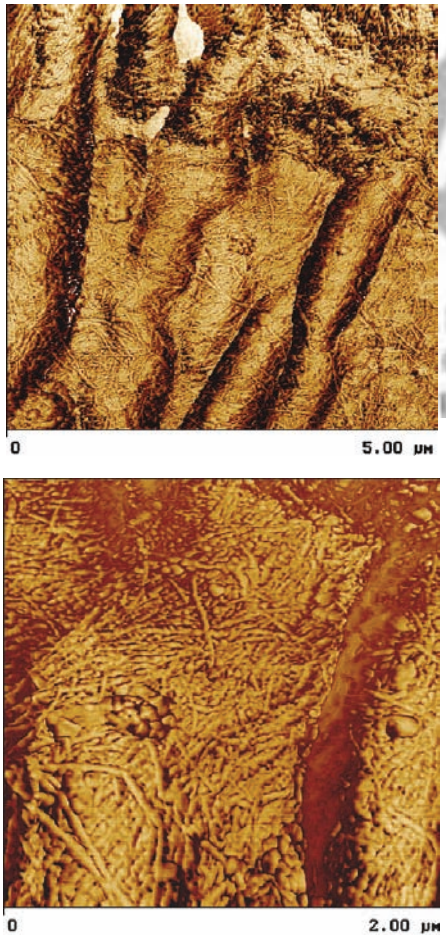

Fig. 6. AFM images using intermittent contact (phase mode) for sisal fibers treated with 40% NaOH in scan size of (a) 5 μm and (b) 2 μm.

Table I. Surface energy of sisal samples and AFM tip.

Samples	γ (mJ/m^2)	γ^d (mJ/m^2)	γ^p (mJ/m^2)
Sisal fibers *in natura*	52.3	41.2	11.1
Sisal fibers treated with NaOH 40%	51.9	38.5	13.3
Benzylated sisal fibers (30 min)	46.7	39.0	7.7
AFM tip (Si_3N_4)*	44.9	39.9	5.0

*Contact angle values were obtained on silicon nitride plates and are agreement with the literature.[43, 44]

The contact angle analysis may provide information about the hydrophilic/hydrophobic behavior of surfaces. By means of the dynamic contact angle, Trejo-O'Reilly et al.[35] studied the deposition of a formamide drop on the surface of paper modified by various chemical agents. The authors calculated surface energies with the Owens-Wendt approach, as well as the distributions of the polar and dispersive components on each material studied. They noted that the untreated cellulose substrate showed high values for both the polar and dispersive components, as expected for surfaces rich in OH groups. With the introduction of non-polar groups, the dispersive contribution remained unaffected, while the polar component suffered a considerable decrease. In the present research, samples of sisal *in natura*, treated with 40% NaOH and benzylated were analyzed with contact angle measurements. Table I shows the results for different samples, these being averages of at least five determinations, with low values of standard deviation (~3%). The polar component apparently decreased in benzylated fibers, compared with the fiber *in natura*, due to the introduction of dispersive substituents in the cellulose chain, decreasing the quantity of hydrogen bonds and generating a hydrophobic material. However, after treatment with 40% NaOH, an increase in the polar component was observed due to the removal of lignin, which is less hydrophilic than cellulose (rich in hydroxyl groups).

These results were corroborated by force curve measurements, which provided the adhesion force between a tip with hydrophobic characteristics and sisal fibers. It is known[36, 37] that the adhesion force depends on the type of materials interacting and the environment, which can even allow for the identification of the materials. To measure the adhesion forces between the AFM tip and the sisal fiber surface, force curves[38] are obtained with the cantilever tip used as a nanometer-scale adhesion tester. The quantity

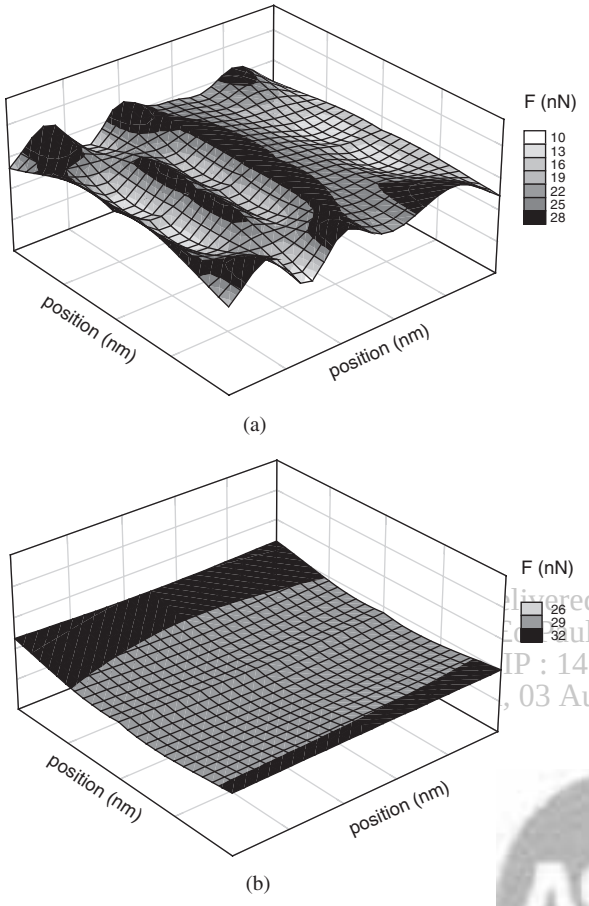

Fig. 7. Adhesion force (F) maps (scan size: 3 μm) of (a) sisal surfaces treated with 40% NaOH and (b) benzylated sisal for 0.5 hour.

measured is the force required to remove the tip from intimate contact with the fiber surface. The pull-off force is thus proportional to the local adhesion energy.

The adhesion maps in Figure 7 show the distribution of adhesion force (F) magnitude on sisal fibers. It should be stressed that for a tip and an electrically neutral and non-magnetic substrate, the force between them can be attributed mostly to van der Waals and capillary interactions. The capillary force can be eliminated if an AFM operates either in a vacuum or in a dry environment. If measurements are made under room conditions, the surface of the samples may be covered by a thin water layer and therefore subjected to capillary forces owing to the water meniscus formed around the tip. Thus, capillary forces affect the interaction between the sample surface and the probe; however, it is affected by the wettability of the substrate and the surface of the tip by water. For a hydrophobic substrate, the thickness of the water film formed is very limited, which may result in a relatively small capillary force.

If the surfaces of both substrate and tip are hydrophilic, a larger water meniscus can be formed around the tip, resulting in a strong capillary force. Indeed, our results and those found in the literature show that the adhesion force depends strongly on whether the substrate and the tip are hydrophilic or hydrophobic.[39] Each adhesion map represents a scan range of 3 μm and the adhesion distribution on the surface is associated with the chemical heterogeneity of the surface. The force curve measurements provided further information on the changes caused by benzylation of the sisal fibers.

The map in Figure 7a shows greater chemical heterogeneity for the fiber treated with 40% NaOH, with adhesion forces varying from 10 to 28 nN, whereas the forces for benzylated sisal in Figure 7b ranged from 26 to 33 nN. This result confirms the increase in the work of adhesion due to the decrease in the polar component of surface energy observed in the contact angle analysis. In the case of an AFM tip with high dispersive values of surface energy (hydrophobic), the decrease in the polar component of the sisal fiber will be responsible for a larger adhesion and good affinity between the materials. These results shows that proper treatment applied to the fibers (hydrophilic) could result in a compatible surface with the synthetic matrix (hydrophobic) that improves the quality of the polymer composites.

The degree of compatibility between an AFM tip and sisal fiber can also be evaluated through the application of a harmonic-mean equation that is used to calculate the work of adhesion (ϖ_{ij}) between the tip (i) and the natural fibers (j); hence the interfacial tension (γ_{ij}) is then calculated:[40]

$$\varpi_{ij} = \frac{4\gamma_i^d \gamma_j^d}{\gamma_i^d + \gamma_j^d} + \frac{4\gamma_i^p \gamma_j^p}{\gamma_i^p + \gamma_j^p} \quad (6)$$

$$\gamma_{ij} = \gamma_i + \gamma_j - \varpi_{ij} \quad (7)$$

Low interfacial tension shows good affinity between the materials. Therefore, the low interfacial tension for the benzylated sisal-tip system is indicative of high compatibility,[41] as can be seen in the adhesion force data of Table II. The tip interacts with the benzylated sisal fiber because of its hydrophobic character. In real systems, polymeric materials such as polypropylene (PP) are used in the preparation of plant fiber-polymer matrix composites.[42] In this work, a Si_3N_4 tip was used because both tip and PP ($\gamma_{pp} = 39.3$; $\gamma^d = 35.5$; and $\gamma^p = 3.8$ mJ/m^2) have similar surface energy, which allow a reproduction, at the nanoscale, of the interaction (adhesion) between the plant fiber and synthetic polymer (e.g., PP).

In our experiment the surface energy of the tip, γ_t, is considered constant; therefore, the change in adhesion

Table II. Interfacial tension and adhesion force between tip and fibers.

Systems	Interfacial Tension (mJ/m^2)	Adhesion force (nN)
Sisal fibers *in natura*–AFM tip	2.34	23 ± 2
Sisal fibers treated with NaOH 40%- AFM tip	3.89	25 ± 2
Benzylated sisal fibers (30 min) AFM tip	0.59	30 ± 2

force is a measure of the combination of surface energy of the sample surface and the interfacial energy between the tip and sample surface. Moreover, the properties of the tip contribute to the adhesion force. In order to eliminate possible changes that could affect the interaction between the tip and surface, we use the same tip and the experiments are carried out within a short period of time.

Finally, the adhesion force measured by AFM pointed to considerable decrease in the polar component of the fiber surface energy after benzylation, which is consistent with the data from angle contact measurements. Therefore, the force curve measurements appear to be promising to evaluate changes in surface energy of natural fibers, which is the main parameter governing the wettability and adhesion properties on polymer composites. The error in the AFM measurements is often significant, up to 15% of the reported value. Therefore, a more detailed study concerning the reason for the discrepancy between solid-vapor surface energy values from contact angle and pull-off force measurements should be performed.

4. CONCLUSIONS

This paper confirms that AFM is useful to evaluate changes in morphology and adhesion resulting from chemical treatment on sisal fibers. AFM and SEM images indicated that sisal fibers consist of bundles of fibers (∼10 μm) that contain aligned microfibrils (∼300 nm), formed by randomly distributed nanofibrils (∼20 nm). AFM images revealed that after incorporation of benzyl groups for 0.5 hour the microfibrils developed a globular morphology (∼120 nm) without losing totally their fibrillar structure. After 2 hours of benzylation, however, only the globular morphology was observed. Measurements of force curves proved that the adhesion force between the sisal fiber and AFM tip increased significantly with benzylation since the tip has a hydrophobic character, which demonstrated the importance of benzylation to decrease the polar component of the fibers. Measurements of contact angle indicated that low levels of benzylation changed the wettability of the fibers, decreasing their surface energy. This was due to the presence of benzyl groups on the sisal surface, which caused the polar contribution to decrease. The results indicated that AFM could spatially map the heterogeneity of the fiber surface with nanometer resolution, supplying useful information about the adhesive characteristics of natural fibers. We believe that studies such as the one presented here may help evaluate interfacial adhesion between the matrix and the fiber at the nanoscale.

Acknowledgments: The authors are grateful to CNPq, FAPESP, and MCT/CNPq (Nanobiotechnology network) for the financial support, and to Embrapa for the facilities. They are also indebted to Prof. Alessandro Gandini (INPG-France) for the contact angle measurements.

References and Notes

1. A. Leão, F. Carvalho, and E. Frollini, *Lignocellulosic-Plastics Composites*, USP/UNESP, São Carlos (**1997**).
2. L. Y. Mwaikambo and M. P. Ansell, *J. Appl. Polym. Sci.* 84, 2222 (**2002**).
3. M. L. O. D'Almeida, Celulose *e Papel: tecnologia de fabricação de pasta celulósica*, São Paulo, IPT (**1988**), Vol. 1, p. 559, 2nd edn.
4. R. Pereira, S. P. Campana Filho, A. A. S. Curvelo, and A. Gandini, *Cellulose* 4, 21 (**1997**).
5. F. C. Ferreira, A. A. S. Curvelo, and L. H. C. Mattoso, *J. Appl. Polym. Sci.* 89, 2957 (**2003**).
6. A. L. Da Róz and A. A. S. Curvelo, *J. Thermal Anal. Calorymetry* 75, 429 (**2004**).
7. S. Iannace, R. Ali, and L. Nicolais, *J. Appl. Polym. Sci.* 19, 1084 (**2001**).
8. K. C. M. Nair, S. M. Diwan, and S. Thomas, *J. Appl. Polym. Sci.* 60, 1483 (**1996**).
9. J. R. M. Almeida, *J. Mater. Sci. Lett.* 2, 578 (**1991**).
10. K. G. Satynarayana, K. Sukumaran, P. S. Mukherjee, C. Pavithran, and S. G. K. Pillai, *Cem. Concr. Compos.* 12, 117 (**1990**).
11. M. A. Martins and L. H. C. Mattoso, *J. Appl. Polym. Sci.* 91, 670 (**2004**).
12. K. Joseph, S. Thomas, and C. Pavithran, *Polymer* 37, 5139 (**1996**).
13. D. K. Owens and R. C. Wendt, *J. Appl. Polym. Sci.* 13, 1741 (**1969**).
14. K. Grundke, T. Bogumil, C. Werner, A. Janke, K. Poschel, and H.-J. Jacobash, *Colloids Surf. A* 116, 79 (**1996**).
15. Y.-K. Lee, H.-J. Kim, M. Rafailovich, and J. Sokolov, *Int. J. Adhes. Adhes.* 22, 375 (**2002**).
16. S. Biggs and G. Spinks, *J. Adhesion Sci. Technol.* 12, 461 (**1998**).
17. F. L. Leite, F. C. Ferreira, P. S. P. Herrmann, and L. H. C. Mattoso, In *Proceedings of the VIII Simposio Latinoamericano de Polímeros, SLAP' SIAQ* (**2002**), p. 278.
18. G. Binnig, C. Quate, and Ch. Gerber, *Phys. Rev. Lett.* 56, 930 (**1986**).
19. T. D. Downing, R. Kumar, W. M. Cross, L. Kjerengtroen, and J. J. Kellar, *J. Adhesion Sci. Technol.* 14, 1801 (**2000**).
20. P. Nygard, K. Grundke, E. Mader, and C. Bellmann, *J. Adhes. Sci. Technol.* 16, 1781 (**2002**).
21. J. A. A. Crossley, C. T. Gibson, L. D. Mapledoram, M. G. Huson, S. Myhra, D. K. Pham, C. J. Sofield, P. S. Turner, and G. S. Watson, *Micron* 31, 659 (**2000**).
22. S. J. Hanley and D. G. Gray, *J. Pulp Pap. Sci.* 25, 196 (**1999**).
23. L. Pang and D. G. Gray, *J. Pulp Pap. Sci.* 24, 369 (**1998**).
24. T. Furuta and D. G. Gray, *J. Pulp Pap. Sci.* 24 , 320 (**1998**).
25. J. A. Irvine, E. D. Aston, and J. C. Berg, *Tappi J.* 82, 172 (**1999**).
26. F. L. Leite, A. Riul, Jr., and P. S. P. Herrmann, *J. Adhes. Sci. Tech.* 17, 2141 (**2003**).
27. H.-J. Butt, A. Doppenschimidt, G. Huttl, E. Muller, and O. I. Vinogradova, *J. Chem. Phys.* 113, 1194 (**2000**).
28. J. Vesenka, S. Manne, R. Giberson, T. Marsh, and E. Henderson, *Biophys. J.* 65, 992 (**1993**).
29. M. G. Goh, D. Juhue, O. M. Leung, Y. Wang, and M. A. Winnik, *Langmuir* 9, 1319 (**1993**).
30. G. W. Stachowiack and A. W. Batchelor, *Engineering Tribology*, Elsevier, Amsterdam (**1993**).
31. P. Aurenty, V. Lanet, A. Tessandro, and A. Gandini, *Rev. Sci. Instrum.* 68, 1801 (**1997**).
32. J. C. Roberts, The Chemistry of Paper, The Royal Society of Chemistry, Cambridge (**1996**).
33. R. Garcia and R. Pérez, *Surf. Sci. Rep.* 47, 197 (**2002**).
34. E. Sjostrom, Wood Chemistry Fundamentals and Applications, Academic Press, USA (**1981**).

35. J. A. Trejo-O'Reilly, J. Y. Cavaillé, M. Paillet, A. Gandini, P. Herrera-Franco, and J. Cauich, *J. Polym. Compos.* 21, 65 (**2000**).
36. T. Nakagawa, K. Ogawa, T. Kurumizawa, and S. Ozaki, *Jpn. J. Appl. Phys.* 32, 924 (**1993**).
37. C. D. Frisbie, L. F. Rozsnyai, A. Noy, M. S. Wrighton, and C. M. Lieber, *Science* 265, 2071 (**1994**).
38. F. L. Leite and P. S. P. Herrmann, *J. Adhes. Sci. Technol.* 19, 365 (**2005**).
39. M. Binggeli and C. M. Mate, *Appl. Phys. Lett.* 65, 415 (**1994**).
40. S. Wu, Polymer Interface Adhesion, Marcel Dekker, New York (**1982**).
41. J. Israelachvili, Intermolecular and Surface Forces, Academic Press, New York (**1995**).
42. J. M. Felix and P. Gatenholm, *J. Appl. Polym. Sci.* 42, 609 (**1991**).
43. C. Jacquot and J. Takadoum, *J. Adhes. Sci. Tech.* 15, 681 (**2001**).
44. J. Li and M. Hattori, *Thermochim. Acta* 88, 267 (**1985**).

Received: 10 October 2005. Revised/Accepted: 13 February 2006.